Journal of Systems Engineering and Electronics
Vol. 32, No. 6, December 2021, pp.1381 – 1393

A method of line spectrum extraction based on target radiated spectrum feature and its post-processing

DAI Wenshu[1,*], ZHENG Enming[2], and BAO Kaikai[3]

1. Key Laboratory of Instrumentation Science & Dynamic Measurement, North University of China, Taiyuan 030006, China; 2. Institute of Acoustics, Chinese Academy of Sciences, Beijing 100190, China; 3. Northern Institute of Automatic Control Technology, Taiyuan 030051, China

Abstract: To improve the ability of detecting underwater targets under strong wideband interference environment, an efficient method of line spectrum extraction is proposed, which fully utilizes the feature of the target spectrum that the high intense and stable line spectrum is superimposed on the wide continuous spectrum. This method modifies the traditional beam forming algorithm by calculating and fusing the beam forming results at multi-frequency band and multi-azimuth interval, showing an excellent way to extract the line spectrum when the interference and the target are not in the same azimuth interval simultaneously. Statistical efficiency of the estimated azimuth variance and corresponding power of the line spectrum band depends on the line spectra ratio (LSR) of the line spectrum. The change laws of the output signal to noise ratio (SNR) with the LSR, the input SNR, the integration time and the filtering bandwidth of different algorithms bring the selection principle of the critical LSR. As the basis, the detection gain of wideband energy integration and the narrowband line spectrum algorithm are theoretically analyzed. The simulation detection gain demonstrates a good match with the theoretical model. The application conditions of all methods are verified by the receiver operating characteristic (ROC) curve and experimental data from Qiandao Lake. In fact, combining the two methods for target detection reduces the missed detection rate. The proposed post-processing method in 2-dimension with the Kalman filter in the time dimension and the background equalization algorithm in the azimuth dimension makes use of the strong correlation between adjacent frames, could further remove background fluctuation and improve the display effect.

Keywords: towed linear array sonar, target radiated noise spectrum, line spectra level ratio (LSR), receiver operating characteristic (ROC) curve, post-processing.

DOI: 10.23919/JSEE.2021.000118

Manuscript received March 06, 2020.

*Corresponding author.

This work was supported by the National Natural Science Foundation of China (51875535) and the Natural Science Foundation for Young Scientists of Shanxi Province (201701D221017;201901D211242).

1. Introduction

Digital multi-beam passive sonar detects remote underwater targets by receiving and processing the noise radiated from the targets. The high frequency band of the radiated noise of the targets is considerably suppressed and attenuated during the signal transmission [1−3]. The low frequency band is suppressed for vibration reduction technology. Thus the signal-to-noise ratio (SNR) of the continuous spectrum received by the passive sonar is very low. Previous research [4−7] pointed out that the current vibration reduction technology cannot suppress the resonance sound radiation induced by the relative motion between the fluid and the targets. And the inertia and working conditions of the targets are relatively stable, resulting in that a series of featured line spectra below 1 kHz superimposes on a continuous spectrum and the line spectra ratio (LSR) of the featured line spectrum is usually 10−25 dB higher than the continuous spectrum.

Traditionally, the passive sonar adopts a robust low-frequency wideband energy integration algorithm and a bearing and time record (BTR) image in the beam domain to detect remote underwater targets [8−10]. However, the anti-jamming performance is poor. Scholars proposed many methods to increase the detection performance of remote underwater targets, which can be sorted into two categories.

(i) Interference suppression methods

Liang et al. suppressed interference using null technology based on spatial filtering [11]. The interference was reconstructed using an inverse beam forming [12,13]. However, the distortion of the array elements often makes the reconstructed interference inaccurate and the interference suppression ability get worse. The weak targets are sometimes submerged by side lobes [14,15]. Yang proposed a low side lobe robust time-domain wideband adaptive beam forming algorithm which can achieve low

side lobe level performance [16]. However, interference suppression performance is low with coherent wideband interference [16−18]. Maragatham et al. proposed a histogram background equalization method to suppress interference and noise [19]. Bao et al. removed the noise interference of the patches using median filtering and threshold analysis [20]. However, these methods bring in snowflake outliers and result in a failure to detect the remote underwater targets.

(ii) Line spectrum detection methods

Li derived that the gain of the narrowband detection was better than the wideband detection method [21]. However, the conclusion is not extended to the multi array and the beam domain. Line spectrum detection methods based on narrow band detection can make full use of the high intensity and stability of the featured line spectrum and achieve high detection gain. However, the beam output of the line spectrum needs to be extracted. Fast Fourier transforms (FFT) and the adaptive line enhancement (ALE) algorithm cannot detect the position of the line spectrum accurately in low signal-to-noise ratio [22−24]. An azimuth stability fusion algorithm was proposed according to the stable azimuth statistics [25−28]. Chen et al. used the frequency statistics to extract the line spectrum beam output [29]. These methods do not utilize intensity stability, and the azimuth or frequency variance statistics cannot be used in the presence of wideband interference with comparable coherent frequencies.

In order to improve the ability of detecting remote underwater targets under strong wideband coherent interference based on narrowband detection, a line spectrum extraction method of multi-azimuth interval and multi-frequency is proposed. The critical LSR is derived by extending the detection gain theory to multi array and beam domain. The improvement of the detection performance by adjusting the LSR above the continuous spectrum is analyzed in the receiver operating characteristic (ROC) charts. The 2-dimensional post processing method with the Kalman filter in the time dimension and the background equalization algorithm in the azimuth dimension spatial domain is designed to solve the problem of snowflake outliers. The proposed method can make full use of the correlation between the target's information in the multi-frame BTR to distinguish the target from the background noise.

2. Line spectrum extraction method of multi-azimuth interval and multi-frequency beam output statistics

Considering the simplified model of the target radiation, the signal $s(t)$ is in the form of the line spectrum of a high LSR superimposed on a wideband continuous spectrum in (1).

$$\begin{cases} s_l(t) = A\cos(2\pi f_l t + \varphi) \\ s(t) = s_l(t) + s_c(t) \\ x_n(t) = s(t + \tau_n(\theta)) + \text{noise}_n(t) \end{cases} \tag{1}$$

where f_l is the featured line frequency, φ is the initial phase. $A = 10^{\frac{\text{LSR}}{20}} / \sqrt{B}$, which is relevant to the LSR and bandwidth of the band pass filter B. $s_c(t)$ is the wideband continuous spectrum. $s_l(t)$ is the line spectrum. According to parallel wave approximation for far field targets, the signal received by each element of a linear array is $x_n(t)(n \in [1, N])$. N is the number of array elements. $\tau_n(\theta)$ is the time delay corresponding to azimuth θ of the nth element. $\text{noise}_n(t)$ is the environmental white noise received by the nth element at the same time.

For signal $x_n(t)$ received in each element, beam forming in the frequency domain is performed. First, the wideband frequency is divided into M, noted as $f_j(j \in [1, M])$. L is the number of preset beam azimuth, noted as $\theta_i(i \in [1, I])$. FFT analysis and phase compensation get the beam output matrix $\boldsymbol{Q}$ of each sub band in (2). The ith column and jth row $P(f_j, \theta_i)$ is the beam domain output of the subband f_j and the preset azimuth θ_i. For each row of matrix $\boldsymbol{Q}$, the azimuth corresponding to the maximum value $P(f_j, \theta_i)$ is the azimuth estimation of that subband denoted by $\hat{\theta}(f_j)(j \in [1, M])$. For subbands of noise, azimuth estimation $\hat{\theta}(f_j)$ is random whereas the azimuth estimation $\hat{\theta}(f_l)$ is stable for target line spectrum subband.

$$\boldsymbol{Q} = \begin{pmatrix} P(f_1,\theta_1) & P(f_1,\theta_2) & \cdots & P(f_1,\theta_{I-1}) & P(f_1,\theta_I) \\ P(f_2,\theta_1) & P(f_2,\theta_2) & \cdots & P(f_2,\theta_{I-1}) & P(f_2,\theta_I) \\ \vdots & \vdots & \ddots & \vdots & \vdots \\ P(f_{M-1},\theta_1) & P(f_{M-1},\theta_2) & \cdots & P(f_{M-1},\theta_{I-1}) & P(f_{M-1},\theta_I) \\ P(f_M,\theta_1) & P(f_M,\theta_2) & \cdots & P(f_M,\theta_{I-1}) & P(f_M,\theta_I) \end{pmatrix} \tag{2}$$

The above procedures are repeated for K times to analyze the azimuth estimation statistics of each subband. Thus for each subband, there will be K estimations $\hat{\theta}_k(f_j)$ $(j \in [1, M], k \in [1, K])$. Calculate the azimuth estimation variance of each band $\sigma_\theta(f_j)(j \in [1, M])$. The $\sigma_\theta(f_l)$ of the line spectrum is small and $\sigma_\theta(f_j)$ of the noise subband $j \neq l$ is large. The traditional wideband energy integration method directly sums all $P_k(f_j, \theta_i)$ in matrix $\boldsymbol{Q}_k(k \in [1, K])$ to get the beam output of the preset azimuth:

$$\text{Pow}_{\text{wide}}(\theta_i) = \sum_{j=1}^{M} \sum_{k=1}^{K} |P_k(f_j, \theta_i)|^2 \ , \quad i \in [1, I] \ . \tag{3}$$

The assumed line spectrum subband detection method sums line $P_k(f_l, \theta_i)$ in matrix $\boldsymbol{Q}_k(k \in [1, K])$ to get the beam output of the preset azimuth:

$$\mathrm{Pow}_l(\theta_i)=|\sum_{k=1}^{K}P_k(f_l,\theta_i)|^2,\quad i\in[1,I]. \tag{4}$$

The line spectrum detection results $\mathrm{Pow}_j(\theta_i)(j\neq l, i\in[1,I])$ of other subbands just replace l in (4) with j. So far, signals in the time domain have been transformed into the spatial domain. The output beam value corresponding to target azimuth estimation takes the shape of a bright path as time goes on in the bearing and time record image.

The above two methods based on beam forming enhances the SNR, but cannot extract $\mathrm{Pow}_l(\theta)$ from $\mathrm{Pow}_j(\theta)(j\in[1,M])$ by searching the maximum of the beam output of all frequency bands when wideband interference arises, and the beam output corresponding to the interference azimuth may be larger than the maximum of $\mathrm{Pow}_l(\theta)$. The omnidirectional statistics of the azimuth variance corresponding to the beam output maximum could not be appropriate. To make full use of the azimuth variance statistical information, the K beam output results of multi-bands are used in different azimuth intervals to meet the low SNR condition and are less affected by coherent-interference.

The specific steps as shown in Fig. 1 are as follows.

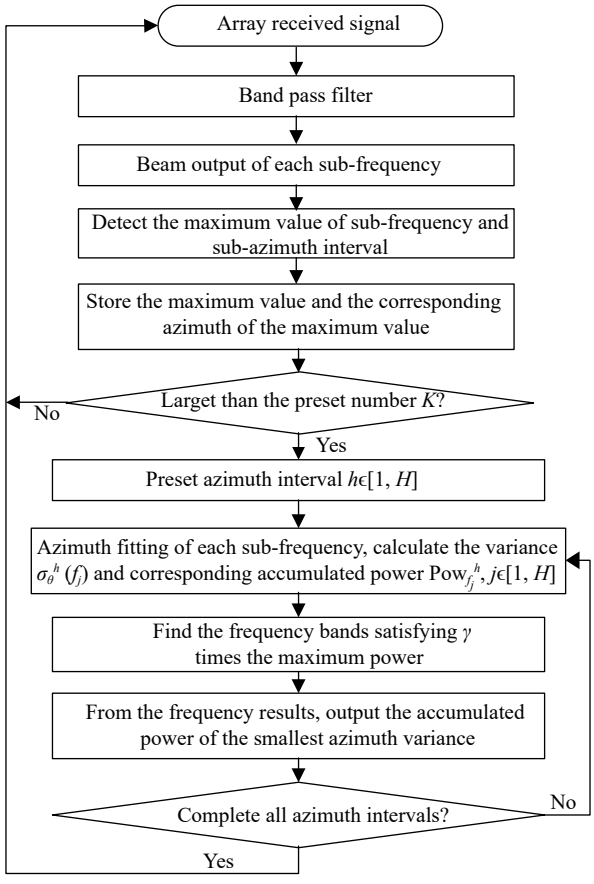

Fig. 1 Flow chart of line spectrum extraction method of multi-azimuth interval and multi-frequency beam output statistics

Step 1 Divide the columns of matrix $\boldsymbol{Q}$ into H intervals. For row j, interval $h,j\in[1,M],h\in[1,H]$, the preset azimuth corresponding to the beam maximum value is regarded as the target azimuth estimation of the current azimuth interval. These procedures are repeated for K times continuously. The azimuth estimation $\hat{\theta}_k^h(f_j)$ and the maximum value $\hat{P}_k^h\left\{f_j,\hat{\theta}_k^h(f_j)\right\}(k\in[1,K])$ of H intervals are recorded respectively.

Step 2 Calculate the azimuth estimation variances of each azimuth interval $\sigma_\theta^h(f_j)(h\in[1,H])$ for the jth subband $j\in[1,M]$. Accumulate the beam output $\hat{P}_k^h(f_j,\hat{\theta}_k^h(f_j))$ according to (5) as the power of the h interval and j subband.

$$\mathrm{Pow}_{f_j}^h=|\sum_{k=1}^{K}\hat{P}_k^h(f_j,\hat{\theta}_k^h(f_j))|^2 \tag{5}$$

Step 3 Extract the beam output of a certain subband based on the recorded azimuth variance and power information of all bands and intervals. The power of the chosen subband ξ is greater than γ times the maximum of all subbands $\mathrm{Pow}_{f_j}^h$ but the estimated azimuth variance is the minimum, as shown in (6). γ represents empirical parameters. This step aims to determine which subband beam will ultimately be output. For azimuth interval h, the unknown line spectrum band will be chosen when strong wideband interference is not in the azimuth interval where the target is located. The K fusion result of line spectrum band $\mathrm{Pow}_{\mathrm{MAMF}}(\theta)$ can be output as one frame.

$$\begin{aligned}&\xi=\min_j\sigma_\theta^h(f_j)\\&\text{s.t. }\mathrm{Pow}_{f_\xi}^h>\gamma\max_j(\mathrm{Pow}_{f_j}^h),\quad j\in[1,M]\\&\mathrm{Pow}_{\mathrm{MAMF}}^h(\theta_i)=|\sum_{k=1}^{K}P_k^h(f_\xi,\theta_i)|^2,h\in[1,H];\ i\in[1,I]\end{aligned} \tag{6}$$

For a certain frame but different azimuth intervals, different sub-band beam output may be chosen. For a different frame but the target azimuth interval, the chosen subband when the LSR satisfies certain requirement can be always the target line spectrum subband.

3. Wide band energy integration and assumed known line spectrum detection gain analysis

All targets in sonar vision can be fully detected by appropriately choosing the multi-band beam outputs in Section 2. Instead of accumulating the reciprocals of each subband's azimuth variance at the bearing of the maximum beam in the azimuth stability fusion algorithm mentioned in the introduction, the multi-azimuth interval and multi-frequency beam output statistics fusion algorithm extracts

the beam output of the target line spectrum frequency, thus the detection gain is equal to assumed known line spectrum detection under a high LSR. The question is how much the LSR of that line spectrum is higher than the continuous spectrum can bring in the same detection performance whether using wide band energy integration or the assumed known line spectrum method, in other words, how much is the critical LSR. The performance of wideband energy integration and the assumed known line spectrum detection in multi array and beam domain are analyzed below.

3.1 Detection performance of wide band energy integration

As we mentioned previously, the target radiated noise is in the form of line spectrum of high spectra level superimposed on wideband continuous spectrum. The detection gain of the wideband energy integration method can be obtained according to the definition of output SNR for wide band systems in (7) from [21].

$$(\frac{S}{N})_Z = \frac{E_1(Z) - E_0(Z)}{\sigma_0(Z)} \tag{7}$$

where Z in is the test statistic we construct to represent wide band energy integration. $E_1(Z)$ is the mean value of system output when the input are $s(t)$ and noise(t), and $E_0(Z)$ and $\sigma_0(Z)$ are the mean value and standard deviation of system output when the input is just noise(t). The physical meaning is the SNR by calculating output direct current (DC) jump to output fluctuation. If the bandwidth of the band pass filter is B, the total number of independent samples during time T is $M' = 2BT$. When the preset beam azimuth is aligned with the target azimuth, the signal power $p_s(n')$ of N array elements in (9) is aligned in phase after phase compensation but uncorrelated noise $p_n(n')$ in (9) is still out of phase. The output signal power and noise power after beam forming are $N^2\sigma_s^2$ and $N\sigma_n^2$, where σ_s^2 and σ_n^2 are signal power and noise power of each element sensor.

$$Z = \frac{1}{M'}\sum_{n'} p^2(n'), \quad n' \in [1, M'] \tag{8}$$

The mean value of multi array beam output when the signal exists is obtained by (10). The mean value and variance of multi array beam output when the input is just noise(t) are obtained by (11) and (12).

$$p(n') = p_s(n') + p_n(n') \tag{9}$$

$$\mathrm{E}[Z|_{p_s+p_n}] = N^2\sigma_s^2 + N\sigma_n^2 \tag{10}$$

$$\mathrm{E}[Z|_{p_n}] = N\sigma_n^2 \tag{11}$$

$$\sigma^2[Z|_{p_n}] = \frac{2}{M'^2}N^2\sigma_n^4 \tag{12}$$

Thus, the obtained output SNR for wideband energy integration is (13). The system gain represented by logarithm is $5\lg(BT) + 10\lg N$.

$$\frac{\mathrm{E}[Z|_{p_s+p_n}] - \mathrm{E}[Z|_{p_n}]}{\sigma[Z|_{p_n}]} = \frac{N^2\sigma_s^2}{\sqrt{\frac{2}{M'}N\sigma_n^2}} = \sqrt{BT}\cdot N\cdot\frac{\sigma_s^2}{\sigma_n^2} \tag{13}$$

3.2 Detection performance of the assumed known line spectrum

By aligning the center frequency of the narrowband filter with the featured line spectrum frequency and filtering most of the noise by passing only the signal component, the output SNR can be increased.

The principle is a matched filter. The impulse response of the filter is $h(t) = p_s^*(-t)$. The test statistic is calculated by (14) after beam forming. $p_s(t)$ and $p_n(t)$ are in (9).

$$Z(t) = p_s^*(-t) * p(t) = \int_T p_s^*(\tau - t)[p_s(\tau) + p_n(\tau)]\mathrm{d}\tau \tag{14}$$

The filtered signal power of the matched filter is in (15), where $P_s(f)$ here is the spectral density of the line spectrum. $\frac{N\sigma_n^2}{2B}$ is the bilateral spectral density of noise.

$$W_s|_{t=0} = [\int_T p_s^*(\tau)p_s(\tau)\mathrm{d}\tau]^2 = [\int_{-B}^{B}|P_s(f)|^2\mathrm{d}f]^2 \tag{15}$$

The output noise power is obtained by (16). The transfer function $H(f) = P_s{}^*(f)$.

$$W_n = \frac{N\sigma_n^2}{2B}\int_{-B}^{B}|P_s(f)|^2\mathrm{d}f \tag{16}$$

The output SNR is as in (17) where $\int_B|P_s(f)|^2\mathrm{d}f$ is the signal power.

$$\frac{\mathrm{E}[Z|_{p_s+p_n}] - \mathrm{E}[Z|_{p_n}]}{\sigma(Z|_{p_n})} = \frac{W_s}{W_n} = \frac{\int_B|P_s(f)|^2\mathrm{d}f}{\frac{N\sigma_n^2}{2B}} = \frac{2N^2\sigma_s^2BT}{N\sigma_n^2} \tag{17}$$

The input SNR is $\frac{\sigma_s^2}{\sigma_n^2}$. The gain represented by the logarithm is $10\lg(2BT) + 10\lg N$.

3.3 Critical line spectrum LSR analysis

Assume the line spectrum is x dB higher than the continuous spectrum. The critical LSR could be obtained by making the output SNR of different methods equal. The SNR of the wide band continuous spectrum $s_c(t)$ and line spectrum $s_l(t)$ are noted as SNR and SNR_l respectively. The expression of the line spectrum signal is $s_l(t) =$

$A\sin(2\pi f_l t+\varphi)$. The definition of the input SNR of continuous spectrum $s_c(t)$ is $\mathrm{SNR}=10\lg\dfrac{\mathrm{var}(s_c(t)}{\mathrm{var}(\mathrm{noise}(t))}$. And the definition of input SNR of line spectrum $s_l(t)$ is $\mathrm{SNR\_}l=10\lg\dfrac{\mathrm{var}(s_l(t)}{\mathrm{var}(\mathrm{noise}(t))}$. Their relationship is as shown in (18) where B is the system bandwidth. Function var stands for power.

$$\mathrm{LSR}=10\lg\frac{\mathrm{var}(s_l(t))B}{\mathrm{var}(s_c(t))}=\mathrm{SNR\_}l-\mathrm{SNR}+10\lg B \quad (18)$$

According to Sub-section 3.1 and -Sub-section 3.2, the input SNR of the wideband energy integration method is derived from (19) by simplifying (18).

$$\mathrm{SNR\_}w=10\lg\frac{\mathrm{var}(s_c(t)+s_l(t))}{\mathrm{var}(\mathrm{noise}(t))}=10\lg(10^{\frac{\mathrm{SNR}}{10}}+10^{\frac{\mathrm{LSR}+\mathrm{SNR}}{10}-\lg B}) \quad (19)$$

The input SNR of the assumed known line spectrum method also can be derived from (18), that is $\mathrm{SNR\_}l=\mathrm{LSR}+\mathrm{SNR}-10\lg B$. Solving (20) we can get the critical line SLR_0.

$$10\lg(10^{\frac{\mathrm{SNR}}{10}}+10^{\frac{\mathrm{LSR}_0+\mathrm{SNR}}{10}-\lg B})+5\lg(BT)+10\lg N=\mathrm{SNR\_}l+10\lg(2BT)+10\lg N \quad (20)$$

If the line LSR x in f_l band is larger than LSR_0, the multi-azimuth interval and multi-frequency beam output statistics fusion based on the assumed known line spectrum detection method is probably much better. The application condition pends discussion later by the simulation.

4. Kalman filter and background equalization in the beam domain

Because of the non-stationary nature in time and inhomogeneity in space of marine background noise, the output of each frame (transverse) of a BTR image retains the azimuth information of the target whereas the background power is high and fluctuates. Section 2 shows that the beam output of each azimuth interval is determined by the azimuth statistical variance and power characteristics of all subbands. Therefore, the beam output result of adjacent frames for the same azimuth interval may not be the result of the same subband. Even if the target or the interference azimuth is stabilized, the beam output also fluctuates. The correlation of beam output near the target azimuth of adjacent frames is strong and can be processed longitudinally by Kalman filtering while smoothing the residual outliers combined with horizontal background equalization.

4.1 Transverse background equalization algorithm

The beam output of one frame after multi-azimuth interval and multi-frequency beam output statistics fusion is represented as $\mathrm{Pow}_{\mathrm{MAMF}}(\theta_1),\mathrm{Pow}_{\mathrm{MAMF}}(\theta_2),\cdots,\mathrm{Pow}_{\mathrm{MAMF}}(\theta_I)$. To eliminate the edge effect, extend the one-sided W point data from the endpoint to the other side, and the expanded output is $\mathrm{Pow}_{\mathrm{MAMF}}(\theta_{W+1}),\cdots,\mathrm{Pow}_{\mathrm{MAMF}}(\theta_2)$, $\mathrm{Pow}_{\mathrm{MAMF}}(\theta_1),\mathrm{Pow}_{\mathrm{MAMF}}(\theta_2),\cdots,\mathrm{Pow}_{\mathrm{MAMF}}(\theta_I),\mathrm{Pow}_{\mathrm{MAMF}}(\theta_{I-1})$, $\cdots,\mathrm{Pow}_{\mathrm{MAMF}}(\theta_{I-W})$. Restate the expanded output as $\mathrm{Pow}'_{\mathrm{MAMF}}(1),\mathrm{Pow}'_{\mathrm{MAMF}}(2),\cdots,\mathrm{Pow}'_{\mathrm{MAMF}}(I+2W)$. Select $\mathrm{Pow}'_{\mathrm{MAMF}}(i)$ to $\mathrm{Pow}'_{\mathrm{MAMF}}(2W+i)$ $(i\in[1,I])$ with length $2W+1$ once, and arrange from small to large to get $y(1),y(2),\cdots,y(2W+1)$. The median is $y(W+1)$. The truncated average of sequence $y(W+1),\cdots,y(2W+1)$ is

$$\bar{y}=\frac{1}{W+1}\sum_{m=1}^{W+1}y(W+m). \quad (21)$$

The threshold $y_0=\alpha\bar{y}$, α is used to adjust the data rejection threshold. Finally, revise every $\mathrm{Pow}_{\mathrm{MAMF}}(i)$ by (22) to get

$$Z(\theta_i)=\begin{cases}0, & \mathrm{Pow}_{\mathrm{MAMF}}(i)<y_0\\ \mathrm{Pow}_{\mathrm{MAMF}}(i)-\bar{y}, & \text{otherwise}\end{cases} \quad (22)$$

where $Z(\theta_i)$ $(i\in[1,I])$ is the beam output after background equalization. For each frame the processing is along the azimuth, and thus, it is termed transverse background equalization.

4.2 Longitudinal Kalman filtering in the beam domain

Note the observed beam output of azimuth θ_i in frame t of BTR image after transverse background in Sub-section 4.1 as $Z_t(\theta_i)$ $(i\in[1,I])$. The beam output of a given azimuth fits the linear Kalman model in (23), where $P_t(\theta_i)$ is the beam output of azimuth θ_i in frame t, and it can be predicted from frame t−1. $N(\theta_i)$ is the observed noise with variance $\sigma_r^2(\theta_i)$. $U(\theta_i)$ is the state noise with variance $\sigma_q^2(\theta_i)$.

$$\begin{cases}Z_t(\theta_i)=P_t(\theta_i)+N(\theta_i)\\ P_t(\theta_i)=P_{t-1}(\theta_i)+U(\theta_i)\end{cases} \quad (23)$$

Filter the beam output between adjacent frames longitudinally for a given azimuth according to recursion formula in (24) [30]. It removes the outliers left by Sub-section 4.1 and enhances the target trajectory.

$$\begin{cases}\hat{P}_{t|t-1}(\theta_i)=\hat{P}_{t-1|t-1}(\theta_i)\\ M_{t|t-1}(\theta_i)=M_{t-1|t-1}(\theta_i)+\sigma_q^2(\theta_i)\\ G_t(\theta_i)=M_{t|t-1}(\theta_i)[\sigma_r^2(\theta_i)+M_{t|t-1}(\theta_i)]^{-1}\\ \hat{P}_{t|t}(\theta_i)=\hat{P}_{t|t-1}(\theta_i)+G_t(\theta_i)[Z_t(\theta_i)-\hat{P}_{t|t-1}(\theta_i)]\\ M_{t|t}(\theta_i)=[I-G_t(\theta_i)]M_{t|t-1}(\theta_i)\end{cases} \quad (24)$$

where $G_t(\theta_i)$ is the Kalman gain for azimuth θ_i. $\hat{P}_{t|t}(\theta_i)$ is the beam output estimation of frame t, $\hat{P}_{t|t-1}(\theta_i)$ is the beam output prediction from frame t−1. $M_{t|t}(\theta_i)$ is the co-

variance of estimation error. $M_{t|t-1}(\theta_i)$ is the covariance of prediction error.

5. Simulation

As we all know from previous sections, the target radiation is composed of a continuous spectrum and a low frequency line spectrum. The continuous spectrum conforms to a P-order autoregressive (AR) model [3]. Its shape satisfies the characteristics of (25) where f_m decides the bandwidth. f_0 decides the peak location. σ_w^2 is related to the energy of the continuous spectrum. The autocorrelation sequence (26) can be obtained from the inverse Fourier transform of (25). The AR model parameters can be calculated by the Levisohn-Durbin recursive method. Continuous spectrum sequences can be generated by white noise passing though this AR model. The line spectrum of low frequency f_l in (27) is superimposed on the continuous spectrum as shown in (25).

$$P_c(f)=\frac{\sigma_w^2}{2\pi}\left[\frac{f_m}{{f_m}^2+(f+f_0)^2}+\frac{f_m}{{f_m}^2+(f-f_0)^2}\right] \tag{25}$$

$$R_c(\tau)=\mathrm{e}^{-2\pi f_m|\tau|}\cos(2\pi f_0\tau) \tag{26}$$

$$P_l(f)=\sum_{l=1}^{L}A_l^2\delta(f-f_l) \tag{27}$$

A large number of experiments show that the spectrum intensity at only a few frequencies is higher than the continuous spectrum. These frequencies are related to the number of propeller blades, rotational speed and speed of the target. Based on the shaft frequency information, three directed low frequency lines 69 Hz, 87 Hz, and 110 Hz are selected. The order in (25) is 30. Bandwidth f_m is 120 Hz. f_0 is 200 Hz. The average power spectrum of 25 times is shown in Fig. 2, which is very close to the real radiated noise.

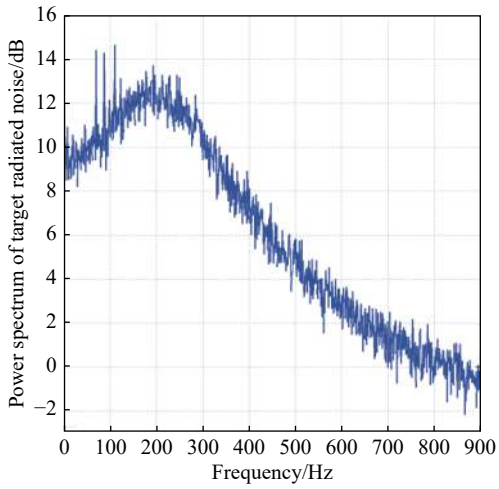

Fig. 2 Power spectrum of target radiated noise from the AR model

5.1 Theoretical detection gain simulation

To verify the detection performance of wideband energy integration and the assumed known line spectrum detection method in Section 3, first simply suppose the target only radiates the line spectrum. The line spectrum frequency is 69 Hz. The number of array elements is 32, and the array spacing is 8 m. Table 1 lists the system gain's variation with integration time T(s), bandwidth B(Hz) and input SNR, according to (18) and (19), SNR_w = SNR_l. The theoretical gain of wide band energy integration in Table 1 is calculated by $5\lg(BT)+10\lg N$, and the theoretical gain of the narrow band line spectrum is calculated by $10\lg(2BT)+10\lg N$. The simulation gain is calculated according to (7).

Table 1 Detection performance of wideband energy integration and the assumed known line spectrum

Input SNR/dB	B/Hz	T/s	Gain (w) in theory/dB	Gain (w) in simulation/dB	Gain (l) in theory/dB	Gain (l) in simulation/dB
−5	190	0.5	24.9	24.94	37.4	37.83
−5	190	1	26.4	26.44	40.4	40.8
−5	140	0.5	24.2	24.27	36.4	36.51
−5	140	1	25.9	25.7	39.1	39.5
−5	110	0.5	23.5	23.75	34.2	35.46
−5	110	1	25.4	25.2	38.2	38.4
−2	190	0.5	25.1	24.9	38.1	37.8
−2	190	1	24.9	27.9	43.1	43.8
−2	140	0.5	24.5	24.2	35.9	36.5
−2	140	1	27.4	27.2	42.4	42.5
−2	110	0.5	23.6	23.7	34.9	35.4
−2	110	1	26.6	26.7	40.9	41.4
1	190	0.5	24.6	24.9	38	37.8
1	190	1	26.5	26.4	41.1	40.8
1	140	0.5	24.4	24.2	37.1	37.5
1	140	1	25.7	25.7	39.9	39.5
1	110	0.5	23.9	23.7	34.9	35.4
1	110	1	25.2	25.2	37.9	38.4

Fig. 3 shows how the SNR gain of the wideband energy integration method (lower curves) and the assumed known line spectrum detection method (upper curves) changes with the band width when the integration time T is set to 1 s and input SNR_w or SNR_l is −2 dB, 1 dB, 3 dB respectively. Fig. 4 shows how the SNR gain of the wideband energy integration method (lower curves) and the narrow band line spectrum detection method (upper

curves) relates to the integration time when the band width is set to 190 Hz in three different input SNR conditions. The simulation results shown in Table 1, Fig. 3 and Fig. 4 are in good agreement with the theoretical calculations.

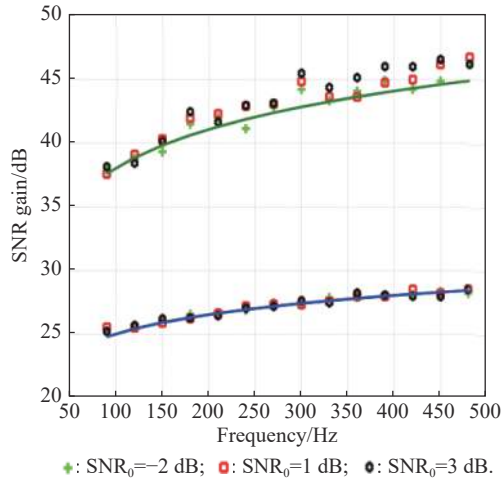

Fig. 3 SNR gain changing with the band width under different input SNRs with wideband energy integration method and assumed known line spectrum detection method

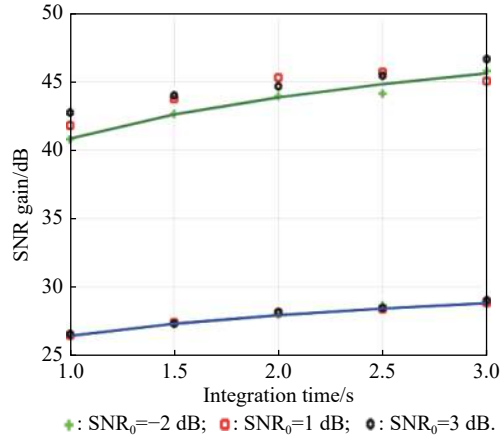

Fig. 4 SNR gain changing with the integration time under different input SNR, with the wideband energy integration method and the assumed known line spectrum detection method

Secondly, target radiation is modeled as low frequency line spectrum superimposed on wide band continuous spectrum which is closer to reality. The array parameters are the same as above. The integration time T=1 s, bandwidth B=190 Hz, The SNR of wideband continuous spectrum SNR remains unchanged at −26 dB, and the LSR changes from 1 dB to 20 dB. It can be seen from Fig. 5 that with the increase of LSR, SNR_l of the assumed known line spectrum detection algorithm noted as LD increases linearly from – 47 dB to −27 dB. And the SNR_w of the wideband detection algorithm noted as WD increases slowly from −25.9 dB to −24 dB, basically unchanged. The output SNR of the assumed known line spectrum detection algorithm increases with the increase of LSR, and the gain is about 40 dB. The output SNR of wideband detection is approximately 26 dB, which is consistent with the theoretical analysis. By fitting the output SNR of the assumed known line spectrum detection and intersecting with the output SNR of the wideband detection algorithm, the critical LSR_0 is approximately 9 dB. When LSR is lower than LSR_0, the variance of the output SNR of the line spectrum detection method is larger. While the LSR is much higher than LSR_0, the variance of the output SNR of the assumed known line spectrum detection method is smaller.

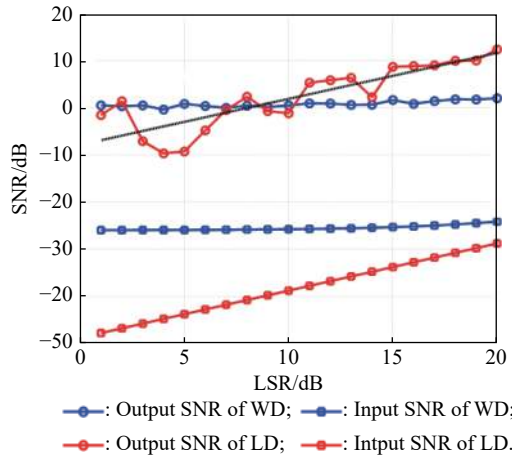

Fig. 5 Output SNR curves changing with line LSR

5.2 Critical LSR_0

In the following, the change law of output SNR with LSR_0, filter bandwidth B and integration time T are studied. When the SNR of the wideband continuous spectrum is −30 dB, the integration time T=1 s, and the pass band B changes from 90 Hz to 490 Hz, It can be seen from the solid line in Fig.6 that the output SNR of wideband detection increases with the increase of bandwidth, basically unchanged when the line spectrum LSR is low, and then increases significantly with the increase of LSR. The output SNR of assumed known line spectrum detection, as shown by the dotted line in Fig.6, increases with the increase of LSR, but does not change with the bandwidth. The intersection in the figure indicates the critical spectrum level of line spectrum required when the output SNR of the two detection algorithms is equal, and the required critical spectrum level increases with the increase of filter bandwidth.

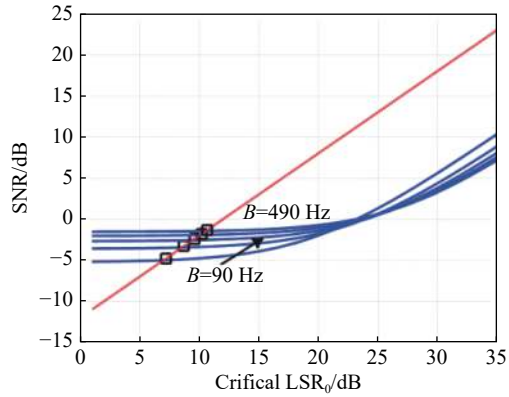

Fig. 6 Change of critical LSR$_0$ with filtering bandwidth

When the input SNR of the wideband continuous spectrum is −30 dB, the filter bandwidth is 190 Hz, and the integration time T changes from 1 s to 10 s. In Fig.7, the solid line is the output SNR of the wideband detection, which is basically unchanged at the lower line spectrum level, but increases with the increase of integration time. When the LSR is higher than 20 dB, it increases significantly with the increase of LSR. The dotted line is the output SNR of the assumed known line spectrum detection, and the output SNR increases with the increase of LSR. The critical spectral level decreases with the increase of integration time.

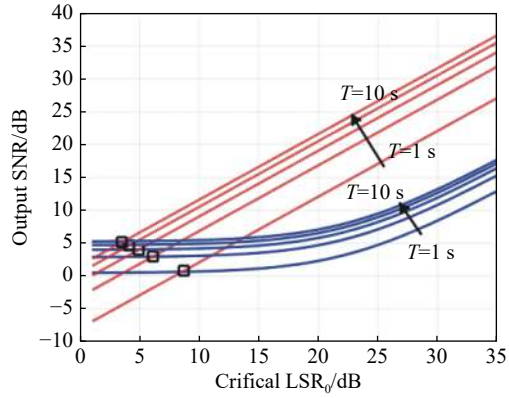

Fig. 7 Change of critical spectral level LSR$_0$ with integration time

5.3 Receiver operating characteristic curve simulation

The requirements of wide-band integral detection, assumed known line spectrum detection and the line spectrum extraction method of multi-azimuth interval and multi-frequency beam output statistics for the input SNR can be seen from the ROC curve, which shows how much SNR the receivers of different algorithms need, and the LSR required by multi-azimuth interval and multi-frequency beam output statistics extraction method. When the phase compensation angle is aligned with the target orientation, a threshold is set for the output signal. If the threshold is exceeded, the judgment of "target" is made. If the threshold is too high, the detection probability and false alarm probability will be low. If the threshold is too low, the detection probability and false alarm probability will be both high. For a specific output SNR, different threshold values correspond to a pair of different detection and false alarm probabilities.

A 32-element linear array with an array spacing of 8 m is set up. The signal is a wideband continuous spectrum with a bandwidth of 10−200 Hz superimposed with a line spectrum signal of 69 Hz. The sampling frequency is 2 kHz. The ROC detection performance of the three algorithms will be simulated. The integration time of wideband detection and assumed known line spectrum detection in 69 Hz is 10 s. The integration time of multi-azimuth interval and multi-frequency beam output statistics extraction method is 1 s. For every subband, 10 s is taken to extract certain subband according to variance statistics of azimuth estimation and its power statistics. The filtering bandwidth is divided into 190 subbands, and 0−180° is divided into four azimuth intervals. The target is located in the second azimuth interval.

When the input SNR of the continuous spectrum is −32 dB, to reach the output SNR represented by the dotted line in Fig.8, the wideband detection algorithm with T=10 s needs to meet the LSR of at least 23 dB. And the assumed known line spectrum detection requires the spectrum level of 18 dB when T=1 s.

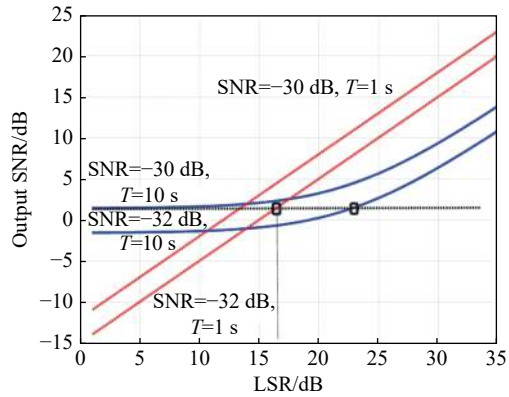

Fig. 8 Determination of LSR$_0$ for line spectrum extraction method of multi-azimuth interval and multi-frequency beam output statistics

From Fig.9, it can be concluded that detection performance of the multi-azimuth interval and multi-frequency beam output statistics extraction method is poor because the false alarm probability of 1 s assumed known line spectrum detection is worse than that of wideband detection.

When the line spectrum level rises to 25 dB, the variance statistics of azimuth estimation and accumulated power of 10 times at azimuth estimation of every subband in the target azimuth interval are as shown in Fig.10

and Fig. 11. The detection probability of the line spectrum when T=1 s increases, and the false alarm probability decreases. The multi-azimuth interval and multi-frequency beam output statistics extraction algorithm can correctly extract 69 Hz beam output in the target azimuth interval, and is close to the detection performance of assumed known line spectrum detection in 69 Hz when T=10 s in Fig. 12.

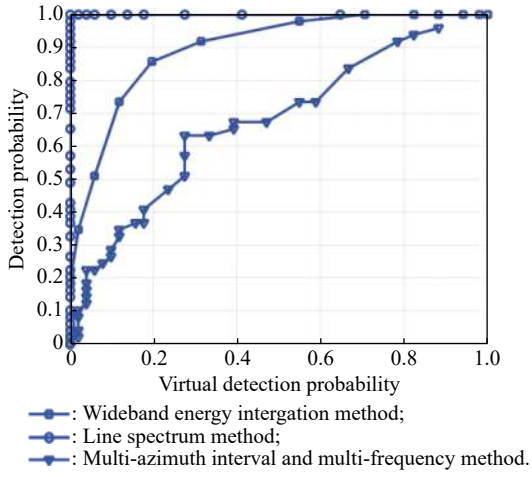

Fig. 9 ROC curves of three algorithms when LSR=18 dB

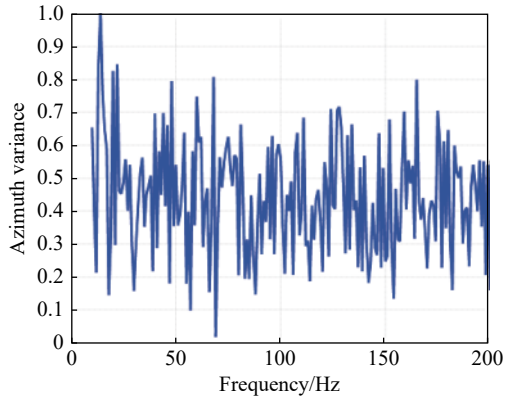

Fig. 10 Variance statistic of 10 s azimuth estimation of every subband in the target azimuth interval

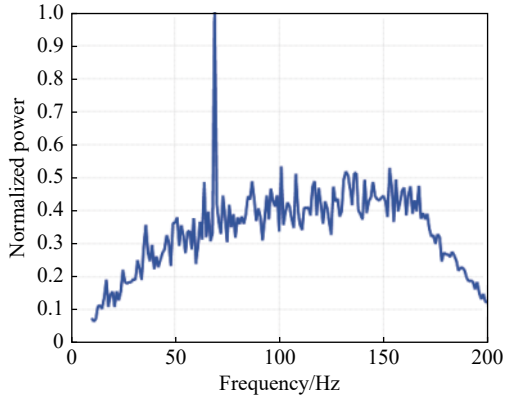

Fig. 11 Accumulated power at 10 s azimuth estimation of every subband in the target azimuth interval

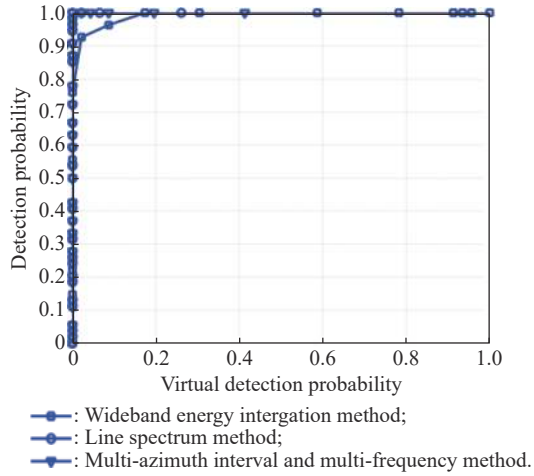

Fig. 12 ROC curves of three algorithms when LSR=25 dB

Therefore, when the LSR is greater than 18 dB until the assumed known line spectrum detection of T=1 s can effectively extract the target line spectrum subband. Although the performance of 10 s wideband energy integration detection is also improved when LSR increases, the performance of multi-azimuth interval and multi-frequency beam output statistics extraction method is near line spectrum detection in 69 Hz of T=10 s .

6. Experimental results

The trial data were obtained at Qiandao Lake, China in November 2012. In the experiment, a 32-element horizontal towed linear array was used to receive signals. The distance between adjacent elements was 8 m, and the endfire direction of towed linear array was 0°. There are two line spectrum targets. The first target with stable line spectra at 69 Hz and 77 Hz of high intensity was moving slowly from 100° to 130° relative to the long linear array. The second line spectrum target was moving slowly at approximately 70° with continuous spectra in the low frequency band of less than 60 Hz. The line spectrum of high intensity is added around 82 Hz. The sampling frequency was 20 kHz; the integral time T was 1 s. The beam domain results were output every 10 s as a frame of the bearing and time map. For convenience, the received data was down sampled and filtered from 40 Hz to 100 Hz. The total observation time was approximately 12 min. The abscissa of the BTR map represents the azimuth of the target relative to the bow, and the ordinate represents the observation time. There were three other strong interferences during the observation time. The first wideband interference at approximately 20°−40° was ship self-noise according to past experience. In addition, there was another obvious strong wideband interference moving at around 145°.

The third wideband interference at 95° did not increase its horsepower until the sixth minute or so. Fig. 13 shows the BTR map of the conventional wideband energy integration method. The background noise is high because of the spatial spectrum leakage. Before 300 s, neither these two weak line targets with high intensity line spectra can be clearly detected by the wide band energy integration method.

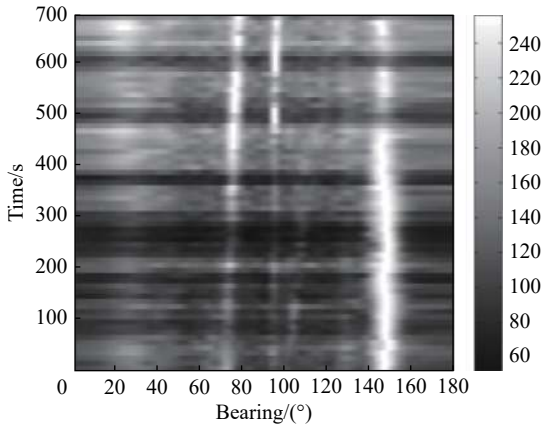

Fig. 13 BTR map of wideband energy integration

By using the existing azimuth variance stability fusion algorithm, Fig. 14 shows that the wideband interference trajectory also can be detected after the azimuth stability fusion algorithm. However, during 70−120 s, only the 69 Hz line target can be detected. During 120−210 s, only the 82 Hz line target can be detected. During 0−70 s and 210−270 s, both two line target lost detection for the accumulative azimuth variance in the line spectrum frequency is too small compared with the accumulative azimuth variance of other frequency band because the wideband interference has a larger SNR. Thus the existence of very strong wideband interference also causes the line spectrum targets missing by using the existing azimuth stability fusion algorithm.

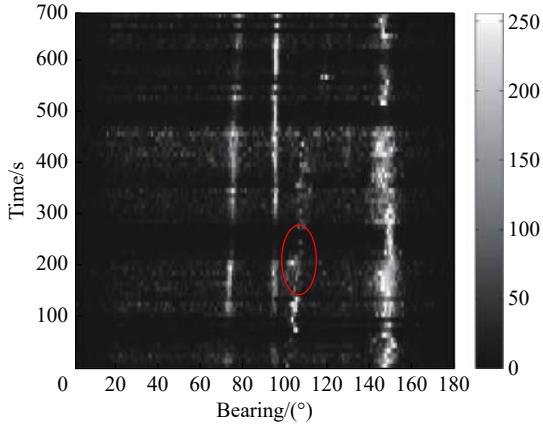

Fig. 14 BTR map of the azimuth stability fusion algorithm

The display effect can further be enhanced by post-processing methods no matter which algorithm is used. Fig. 15 shows the smoother result of wideband energy integration after processed only by Kalman longitudinal filtering. Classic horizontal background equalization removes the broad beam self-ship interference and suppresses the background noise. Fig. 16 shows the target trajectories are obviously enhanced. However, some snow like outliers of the trajectory fracture problems appear. Thus simply use either Kalman longitudinal or horizontal background equalization can not clearly detect the line spectrum target. Fig. 17 shows the wideband energy integration BTR map after post-processed in two dimensions with Kalman longitudinal filtering and horizontal background equalization. Compared with Fig. 13, the target trajectory shows much clearer and the background becomes cleaner, yet one of the line spectrum target of interest is still missing.

Then we try the line spectrum extraction method of multi-azimuth interval and multi-frequency beam output statistics extraction algorithm. Divide the azimuth zone into four intervals, as shown in Fig. 18.

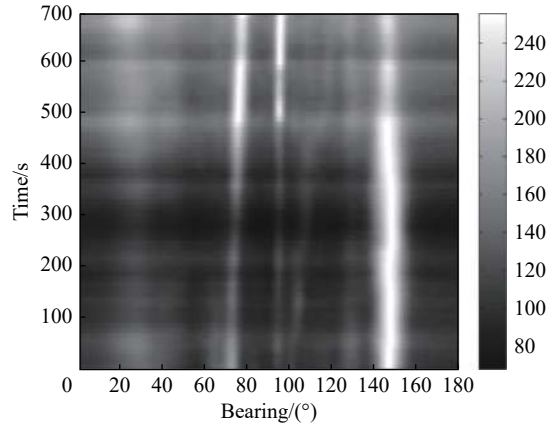

Fig. 15 BTR map of wideband energy integration after Kalman longitudinal filtering

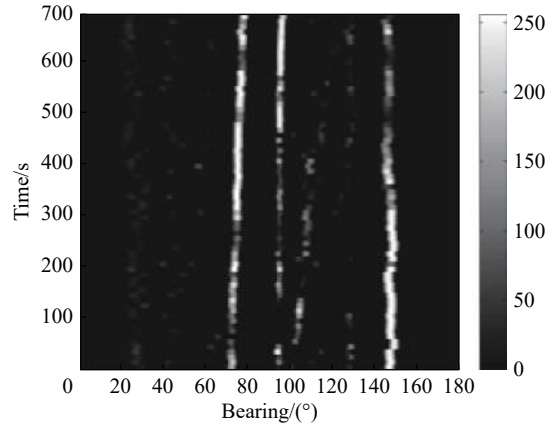

Fig. 16 BTR map of wideband energy integration after horizontal background equalization

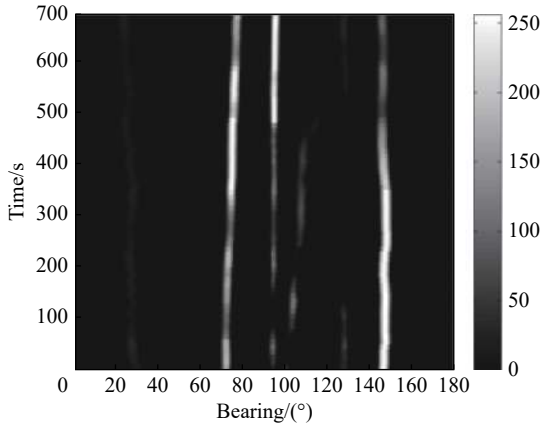

Fig. 17 BTR map of wideband energy integration after Kalman longitudinal filtering and horizontal background equalization

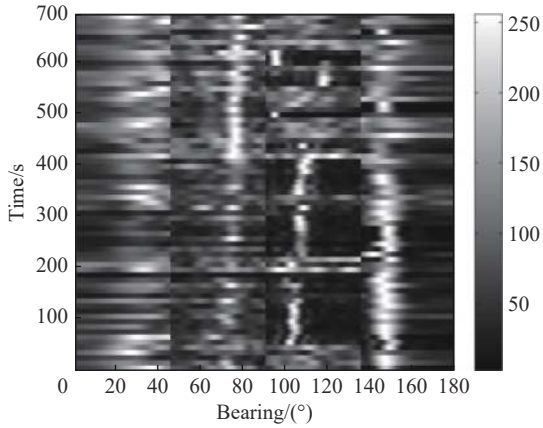

Fig. 18 BTR map of line spectrum extraction method of multi-azimuth interval and multi-frequency beam output statistics

The different subband beam output results of respective azimuth interval were obtained by the line spectrum extraction method raised in Section 2. According to the high output SNR and the critical LSR requirement from Fig. 3, Fig. 4 and Fig. 8, we can see from Fig. 18 that in the third azimuth interval the trajectory of the 69 Hz weak line spectrum target appears, and the output background noise is also low. In the second azimuth interval the trajectory of the 82 Hz line target is also detected. It is necessary to mention that it is not inevitable in some circumstances the azimuth estimation variance does not work. At some certain frames after 450 s in the third azimuth zone, the beam output in 69 Hz of the line spectrum target can not be extracted because the continuous spectrum of the wideband interference were enhanced very high so multiple sources appeared in the same interval. This algorithm can only extract one line spectrum beam output in an azimuth interval.

Because the 82 Hz line target has continuous spectra. Comparing Fig. 13 with Fig. 18, in the second azimuth interval, we can conclude the wideband energy integration method is comparable with the line spectrum detection. Because at each frame the chosen subband output with these two methods, the background level was equivalent. In contrast, the 69 Hz line target located in the third azimuth interval radiated a higher LSR and for most of time was stable. The chosen subband output at each frame was the line spectrum subband. The background level is low. Therefore, the performance of line spectrum detection is much better than the wide band energy integration in this azimuth interval.

Because the same subband was chosen at each frame, the longitudinal fluctuation was correlative. Thus the post processing is essential. Fig. 19 shows the smoother result after just using the Kalman longitudinal filtering according to the correlation of the adjacent frame. However, it introduced blur. While if only horizontal background equalization was applied, flaky interference was removed and snow-like noise and trajectory fracture was added, as illustrated in Fig. 20.

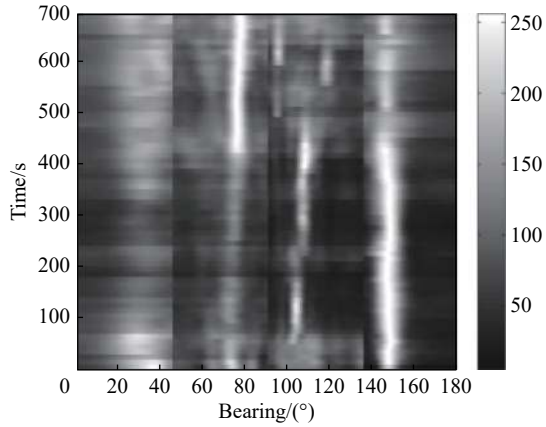

Fig. 19 Kalman longitudinal filtering after line spectrum extraction method of multi-azimuth interval and multi-frequency beam output statistics

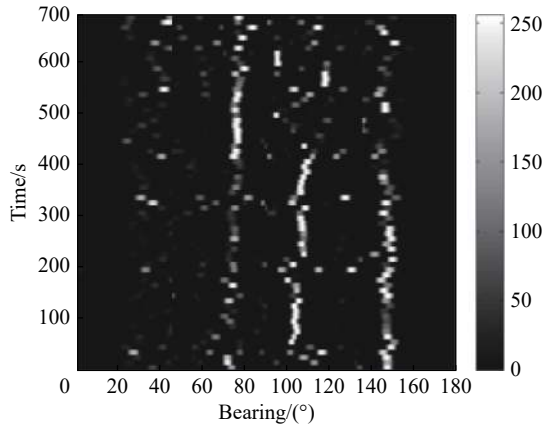

Fig. 20 Horizontal background equalization after line spectrum extraction method of multi-azimuth interval and multi-frequency beam output statistics

Fig. 21 shows the final BTR map of multi-azimuth interval and multi-frequency beam output statistics extraction result after two dimension post processing methods with Kalman longitudinal filtering and horizontal background equalization, on which both two line spectrum targets can be detected in their respective azimuth interval. The display effect becomes much clearer.

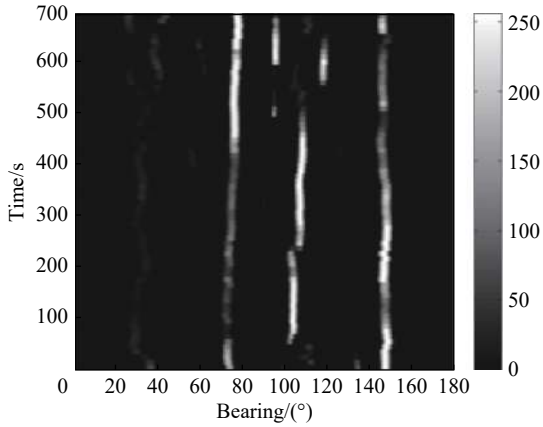

Fig. 21 Kalman longitudinal filtering and horizontal background equalization after line spectrum extraction method of multi-azimuth interval and multi-frequency beam output statistics

7. Conclusions

In this paper, the target radiated signal was modeled as a high intense and stable line spectrum superimposed on the continuous spectrum. The line spectrum extraction method of multi-azimuth interval and multi-frequency beam output statistics was developed by utilizing high LSR feature.

If the input SNR of the target radiated noise is low and the wideband detection algorithm brings high false alarm probabilities, but it contains the line spectrum component of a high spectral level, even if its frequency band is unknown, the line spectrum extraction method of multi-frequency band and multi-azimuth interval statistics can be used to find the unknown frequency band, whose performance is approximately near the assumed known line spectrum detection in the azimuth interval. The proposed line spectrum extraction method will be invalid if multiple sources with comparable beam output in line spectrum band appear in the azimuth interval where the weak target is located.

The azimuth history data processed by all detection methods on BTR maps have the problems of high background noise, serious interference and blurred display. Beam domain horizontal background equalization and Kalman longitudinal filtering making use of the strong correlation between adjacent frames can remove background fluctuation and improve the display.

References

[1] HE C Y. Analysis and evaluation for transient radiated noise of underwater targets. Harbin, China: Harbin Engineering University, 2013. (in Chinese)
[2] WANG D Z, SHANG E C. Underwater acoustics. Beijing: Science Press, 2013. (in Chinese)
[3] BREKHOVSKIKH L, LYSANOV Y. Fundamentals of ocean acoustics. Berlin: Springer-Verlag, 2003.
[4] SPENCE J H, FISCHER R W. Requirements for reducing underwater noise from ships. IEEE Journal of Oceanic Engineering, 2017, 42(2): 388–398.
[5] BARTEL T, HEROLD S, INFANTE et al. Active vibration reduction of ship propulsion systems. Proc. of the Joint Conference on Acoustics, 2018: 1−6.
[6] OVALLE D, GARCIA-PELAEZ J. Minimizing underwater noise generated by submarine maneuvering: an optimal control approach. IEEE Journal of Oceanic Engineering, 2016, 41(2): 362–372.
[7] LI Q H, LI M, CHEN X H, et al. The interference characteristic of platform and towed body noise in shallow water for active/passive towed array sonar. Proc. of the International Conference and Exhibition on Underwater Acoustics, 2013: 213−220.
[8] ALCANTARA E, ATLAS L, ABADI S. Comparing frequency-difference beamforming and delay-and-sum beamforming as an estimator of direction-of-arrival. The Journal of the Acoustical Society of America, 2016, 140(4): 30.
[9] HUI J. Research on passive detection parameter measurement technology based on single vector sensor. The Journal of the Acoustical Society of America, 2017, 142(4): 2587.
[10] HAMID U, QAMAR R A, WAQAS K. Performance comparison of time-domain and frequency-domain beamforming techniques for sensor array processing. Proc. of the International Conference on Applied Sciences & Technology, 2014: 379–385.
[11] LIANG G L, HAN B, FAN Z. Null broadening of near-field adaptive beam forming. Journal of Huazhong University of Science and Technology (Natural Science Edition), 2013, 41(8): 34–39. (in Chinese)
[12] GE S B, CHEN X H, SUN C Y. The Research on the algorithm of inverse beam forming for interference suppression with good robust. Journal of Electronics & Information Technology, 2014, 37(2): 380–384. (in Chinese)
[13] LI Y, SUN C Y, WEI C H, et al. Real-time cancellation of directional wideband interference in sonar. Applied Acoustics, 2008, 27(4): 257–263. (in Chinese)
[14] WILSON J H. Applications of inverse beamforming theory. Journal of Acoustical Society of America, 1995, 98(6): 3250–3261.
[15] DAI H Y, LI Y Z, LIU Y, et al. Novel research on main-lobe jamming polarization suppression technology. Science China: Information Sciences, 2012, 42(4): 460–468. (in Chinese)
[16] YANG L. Studies on direction of arrival estimation of underwater targets and robust adaptive beam forming method. Xi'an, China: Northwestern Polytechnical University, 2017. (in Chinese)
[17] LI H B, GUO Y D, GONG J, et al. DOA estimation method for coherent weak signal sources in the presence of strong jamming. Modern Radar, 2012, 34(9): 45–49.
[18] HUANG C. Study of strong coherent interference. Harbin, China: Harbin Engineering University, 2012. (in Chinese)
[19] MARAGATHAM G, PRABU T M. Contrast enhancement

by object based Histogram Equalization. Proc. of the World Congress on Information and Communication Technologies, 2011: 1118−1122.
[20] BAO X Z, CHEN X H, LI Q H. New algorithm for background equalization of bearing/time digital sonar display. Proc. of the International Conference and Exhibition on Underwater Acoustics, 2013: 261−266.
[21] LI Q H. Introduction to sonar signal processing. Beijing: Ocean Press, 1993. (in Chinese)
[22] MA L, GULLIVER TA, ZHAO A B, et al. Underwater broadband source detection using an acoustic vector sensor with an adaptive passive matched filter. Applied Acoustics, 2019, 148: 162–174.
[23] ZHANG J, LI Y A, ALI W, et al. Line spectrum enhancement of underwater acoustic signals using Kalman Filter. Journal of Marine Science and Application, 2020, 19(1): 148–154.
[24] LUO X W, SHEN Z H. A space-frequency joint detection and tracking method for line-spectrum components of underwater acoustic signals. Applied Acoustics, 2020, 172: 107609.
[25] ZHENG E M, YU H B, CHEN X H, et al. Line spectrum detection algorithm based on the phase feature of target radiated noise. Journal of Systems Engineering and Electronics, 2016, 27(1): 72–80.
[26] SONG M Y, LI J Q. Extraction of shaft frequency based on the DEMON line spectrum. The Journal of the Acoustical Society of America, 2018, 144(3): 1944.
[27] HEN X H, YU H B, SUN C Y. A method for detecting and recognizing underwater acoustic target signals. Chinese Patent 101738611A, 2010. (in Chinese)
[28] CHEN X H, YU H B. Research on detection of underwater acoustic signal with unknown frequency. Acta Armamentarii, 2012, 33(4): 471–475. (in Chinese)
[29] CHEN Y, WANG Z J, ZHU D Z. A detecting method for line-spectrum target based on variance-of-frequency weight. Acta Acustica, 2010, 35(1): 76–80. (in Chinese)
[30] GUO X, GE F X, GUO L H. Improved adaptive Kalman filtering and its application in acoustic maneuvering target tracking. Acta Acustica, 2011, 36(6): 611–618. (in Chinese)

Biographies

DAI Wenshu was born in 1987. She received her B.S. degree in ocean technology from Ocean University of China in Qingdao in 2010 and Ph.D. degree in 2015 from the Institute of Acoustics, Chinese Academy of Sciences, Beijing. Now she is a lecturer in North University of China and does research in the Key Laboratory of Instrumentation Science & Dynamic Measurement. She is dedicated to the research of underwater signal processing and detection, array engineering technology, underwater acoustic communication, and water acoustics physics.
E-mail: daiwenshu@nuc.edu.cn

ZHENG Enming was born in 1985. He received his B.S. degree from Harbin Engineering University in 2009 and was recommended to the Institute of Acoustics, Chinese Academy of Sciences (IACAS), Beijing, China. He received his Ph.D. degree in 2014 from IACAS as a first class graduate. Now he is working in the Weak Signal Detection and Processing Laboratory, Institute of Acoustics, Chinese Academy of Sciences, and he is an assistant researcher. His research interests include signal processing and detection, signal processing technology of sound pressure and velocity, array engineering technology, and array signal processing techniques of underwater acoustic communications and positions.
E-mail: zhengenmingioa@163.com

BAO Kaikai was born in 1989. He received his B.S. degree in electronic science and technology from Southwest Jiaotong University, Chengdu, China, in 2011 and M.S. degree in microelectronics and solid-state electronics from University of Chinese Academy of Sciences, Beijing, China, in 2014. His research interests include the development of micro-electro-mechanical systems and underwater wireless sensor networks.
E-mail: baokaikai2007@126.com